tion ratios (*33–36*) yields an initial $^{92}Nb/^{93}Nb$ for the solar system of 1×10^{-5} to 4.6×10^{-5}, if the free decay interval is not considered. Our estimate based on Estacado falls into this range. Taking into account the free decay interval [up to 50 My (*10*)] may further lower the calculated value by a factor of 2 or more. Nonetheless, most production ratio yields of different supernova models (type Ia and type II) are quite similar to our measured value of $1.2 (\pm 0.6) \times 10^{-5}$. Thus, our data provide only limited constraints on the type of supernova that produced the ^{92}Nb initially present in the solar system.

References and Notes

1. F. A. Podosek, T. D. Swindle, in *Meteorites and the Early Solar System*, J. F. Kerridge, M. S. Matthews, Eds. (Univ. of Arizona Press, Tucson, AZ, 1988), pp. 1093–1113.
2. G. J. Wasserburg, in *Protostars and Planets II*, D. C. Black, M. S. Matthews, Eds. (Univ. of Arizona Press, Tucson, AZ, 1985), pp. 703–737.
3. T. D. Swindle, in *Protostars and Planets III*, E. H. Levy, J. I. Lunine, Eds. (Univ. of Arizona Press, Tucson, AZ, 1993), pp. 867–881.
4. F. A. Podosek, R. H. Nichols, in *Astrophysical Implications of the Laboratory Study of Presolar Materials*, T. J. Bernatowicz, E. Zinner, Eds. (API, New York, 1997), pp. 617–647.
5. T. Makino, M. Honda, *Geochim. Cosmochim. Acta* **46**, 565 (1982).
6. D. R. Nethaway, A. L. Prindle, R. A. Van Konyenburg, *Phys. Rev. C* **17**, 1409 (1978).
7. J. Wade, B. J. Wood, *Nature* **409**, 75 (2001).
8. K. P. Jochum, H. M. Seufert, B. Spettel, H. Palme, *Geochim. Cosmochim. Acta* **50**, 1173 (1986).
9. J. F. Minster, C. J. Allègre, *Geochim. Cosmochim. Acta* **46**, 565 (1982).
10. C. L. Harper Jr., *Astrophys. J.* **466**, 437 (1996).
11. Q. Z. Yin *et al.*, *Astrophys. J.* **535**, L49 (2000).
12. C. Muenker *et al.*, *Science* **289**, 1538 (2000).
13. C. Sanloup, J. Blichert-Toft, P. Trélouk, P. Gillet, F. Albarède, *Earth Planet. Sci. Lett.* **184**, 75 (2000).
14. T. Hirata, *Chem. Geol.* **176**, 323 (2001).
15. Details of analytical methods and supplementary data are available on *Science* Online at www.sciencemag.org/cgi/content/full/295/5560/1705/DC1.
16. B. Hattendorf, D. Günther, M. Schönbächler, A. N. Halliday, *Anal. Chem.* **73**, 5494 (2001).
17. Y. Amelin, D. C. Lee, A. N. Halliday, R. T. Pidgeon, *Nature* **399**, 252 (1999).
18. S. K. Sahoo, A. Masuda, *Chem. Geol.* **141**, 117 (1997).
19. C. Göpel, G. Manhes, C. J. Allègre, *Earth Planet. Sci. Lett.* **121**, 153 (1994).
20. I. Leya, R. Wieler, A. N. Halliday, *Lunar Planet. Sci. Conf.* **XXXII**, 1521 (2001).
21. K. Nicolussi *et al.*, *Astrophys. J.* **504**, 492 (1998).
22. M. Schönbächler *et al.*, *Meteorit. Planet Sci.* **36**, A184 (2001).
23. I. Flohs, *Eos* **62**, 17 (1981).
24. B. W. Stewart, D. A. Papanastassiou, G. J. Wasserburg, *Geochim. Cosmochim. Acta* **58**, 3487 (1994).
25. T. R. Ireland, F. Wlotzka, *Earth Planet. Sci. Lett.* **109**, 1 (1992).
26. T. R. Ireland, *Lunar Planet. Sci. Conf. XXXII* **22**, 609 (1991).
27. G. W. Lugmair, A. Shukolyukov, *Geochim. Cosmochim. Acta* **62**, 2863 (1998).
28. D. C. Lee, A. N. Halliday, *Nature* **388**, 854 (1997).
29. S. B. Jacobsen, Q. Z. Yin, *Lun. Planet. Sci. Conf.* **XXXII**, abstract 1961 (2001).
30. Q. Z. Yin, S. B. Jacobsen, J. Blichert-Toft, P. Télouk, F. Albarède, *Lunar Planet. Sci. Conf.* **XXXII**, abstract 2128 (2001).
31. D. L. Lambert, *Astron. Astrophys. Rev.* **3**, 201 (1992).
32. D. D. Clayton, E. Dwek, S. E. Woosley, *Astrophys. J.* **214**, 300 (1977).
33. S. E. Woosley, W. M. Howard, *Astrophys. J. Suppl. Ser.* **36**, 285 (1978).
34. W. M. Howard, B. S. Meyer, S. E. Woosley, *Astrophys. J.* **373**, L5 (1991).
35. W. M. Howard, B. S. Meyer, in *Nuclei in the Cosmos II*, F. Käppeler, K. Wisshak, Eds. (IOP, London, 1993), pp. 575–580.
36. M. Rayet *et al.*, *Astron. Astrophys.* **298**, 517 (1995).
37. R. D. Hoffman, S. E. Woosley, G. M. Fuller, B. S. Meyer, *Astrophys. J.* **460**, 478 (1996).
38. A. G. W. Cameron, in *Protostars and Planets III*, E. H. Levy, J. I. Lunine, Eds. (Univ. of Arizona Press, Tucson, AZ, 1993), pp. 47–73.
39. G. J. Wasserburg, W. A. Fowler, F. Hoyle, *Phys. Rev. Lett.* **4**, 112 (1960).
40. A. G. W. Cameron, *Icarus* **1**, 13 (1962).

41. We thank three anonymous reviewers for their helpful comments, the Museum of Natural History in Paris for provision of the sample of Estacado, R. Hewins for the sample of Vaca Muerta, and Y. Amelin for the terrestrial zircon samples. Supported by Swiss National Fonds and ETH.

22 October 2001; accepted 23 January 2002

Imaging Sites of Receptor Dephosphorylation by PTP1B on the Surface of the Endoplasmic Reticulum

Fawaz G. Haj,[1] Peter J. Verveer,[2] Anthony Squire,[2] Benjamin G. Neel,[1]* Philippe I. H. Bastiaens[2]*

When bound by extracellular ligands, receptor tyrosine kinases (RTKs) on the cell surface transmit critical signals to the cell interior. Although signal termination is less well understood, protein tyrosine phosphatase–1B (PTP1B) is implicated in the dephosphorylation and inactivation of several RTKs. However, PTP1B resides on the cytoplasmic surface of the endoplasmic reticulum (ER), so how and when it accesses RTKs has been unclear. Using fluorescence resonance energy transfer (FRET) methods, we monitored interactions between the epidermal- and platelet-derived growth factor receptors and PTP1B. PTP1B-catalyzed dephosphorylation required endocytosis of the receptors and occurred at specific sites on the surface of the ER. Most of the RTKs activated at the cell surface showed interaction with PTP1B after internalization, establishing that RTK activation and inactivation are spatially and temporally partitioned within cells.

Most peptide growth factors signal through receptor tyrosine kinases (RTKs). Growth factor binding promotes oligomerization of receptors at the plasma membrane, which leads to receptor activation and the phosphorylation of multiple receptor tyrosyl residues. These tyrosyl phosphorylation sites recruit proteins with Src homology 2 and phosphotyrosine-binding domains, thereby assembling multiprotein complexes that propagate the signal. The amount of phosphotyrosine on RTKs, and thus their signaling capacity, is determined by the balance between RTK activity and the activities of specific protein-tyrosine phosphatases (PTPs). Several PTPs have been implicated in RTK dephosphorylation, but exactly how, when, and where RTK inactivation takes place has remained unknown.

To address the spatiotemporal regulation of RTK dephosphorylation, we investigated the interaction between PTP1B and two RTKs, the epidermal growth factor receptor (EGFR) and the platelet-derived growth factor receptor–β (PDGFR). PTP1B is a widely expressed, prototypical nontransmembrane PTP that can dephosphorylate several RTKs, including the EGFR (*1*) and the insulin receptor (IR) (*2*). Indeed, PTP1B-deficient mice are hypersensitive to insulin and show enhanced tyrosyl phosphorylation of the IR in some insulin-responsive tissues (*3*, *4*). Although $PTP1B^{-/-}$ mice show no obvious evidence of increased EGFR or PDGFR signaling, primary and immortalized $PTP1B^{-/-}$ fibroblasts exhibit increased and sustained ligand-induced tyrosyl phosphorylation of the EGFR and PDGFR, indicating that PTP1B may be a biologically relevant EGFR and PDGFR phosphatase (*5*). However, PTP1B is localized exclusively on the cytoplasmic face of the endoplasmic reticulum (ER), by means of a hydrophobic COOH-terminal anchor sequence (*6*, *7*). These findings raise a conundrum: How does an ER-resident phosphatase dephosphorylate RTKs localized on the plasma membrane or in endocytic vesicles?

The steady-state population of complexes between wild-type PTP1B and RTKs is, on average, very low in cells, because PTP1B has a

[1]Cancer Biology Program, Division of Hematology-Oncology, Department of Medicine, Beth Israel–Deaconess Medical Center, Boston, MA 02115, USA. [2]European Molecular Biology Laboratory, Meyerhofstrasse 1, 69117 Heidelberg, Germany.

*To whom correspondence should be addressed. E-mail: bneel@caregroup.harvard.edu (B.G.N.), bastiaen@embl-heidelberg.de (P.I.H.B.)

catalytic constant (k_{cat}) of ~2×10^3 molecules/min (*8*), rendering it difficult to visualize RTK-PTP1B interactions by using optical techniques. The steady-state population of PTP-substrate complexes can be increased substantially by using PTP mutants that retain substrate-binding ability but are catalytically impaired, so-called substrate trapping mutants (*1*, *9*–*11*). Therefore, we examined dynamic RTK-PTP1B interactions in PTP1B$^{-/-}$ fibroblast cell lines reconstituted with the substrate-trapping mutant D181A (PTP1B$^{D/A}$), in which the general acidic residue aspartate 181 is replaced by an alanine (*12*). By imaging fluorescence resonance energy transfer (FRET) between transiently expressed RTK–green fluorescent protein (GFP) fusions and sulfoindocyanine (Cy3)-conjugated monoclonal antibodies to PTP1B (Cy3-FG6), the sites of RTK-PTP1B$^{D/A}$ interaction, and thus of RTK dephosphorylation within the cell, can be mapped. As controls, similar experiments were carried out with PTP1B$^{-/-}$ fibroblasts reconstituted with wild-type PTP1B (WT PTP1B).

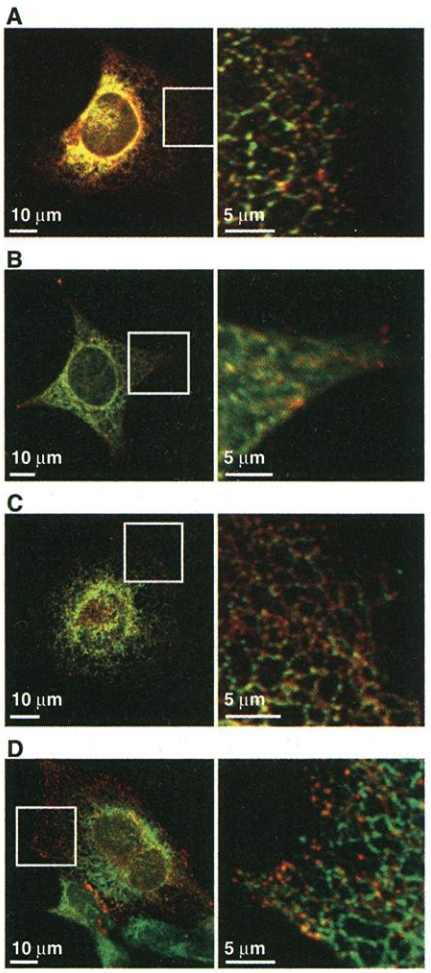

Fig. 1. Localization of PTP1B$^{D/A}$ in punctate structures on the ER. WT PTP1B- and PTP1B$^{D/A}$-reconstituted cells growing on cover slips were deprived of serum for 4 to 6 hours and stimulated with EGF (100 ng/ml) for 15 min. The cells were fixed in methanol at −20°C, incubated with Cy3-labeled monoclonal antibodies to PTP1B (Cy3/FG6) (five Cy3 molecules per antibody) and rabbit polyclonal antibodies to the ER-resident protein TRAP-α, and then incubated with Cy5-conjugated goat antibodies to rabbit immunoglobulin G (Jackson ImmunoResearch Laboratories, West Grove, PA). Images of whole cells (left column) and the indicated (boxed) magnified areas (right column) were acquired with a confocal laser scanning microscope (Leica TCS SP2, Leica, Wetzlar, Germany), equipped with a 63×/1.3 NA oil immersion lens, by using 543-nm (Cy3) and 633-nm (Cy5) laser lines. Unstimulated WT PTP1B- (**A**) or PTP1B$^{D/A}$-reconstituted cells (**B**) and stimulated WT PTP1B- (**C**) or PTP1B$^{D/A}$-reconstituted cells (**D**) were stained for PTP1B (red) and TRAP-α (green). PTP1B and the ER marker colocalize extensively (orange/yellow) in cells expressing either the WT or mutant form of PTP1B. Comparable staining patterns were observed for PDGFR-GFP–transfected cells after PDGF stimulation [Web fig. 1 (*13*)].

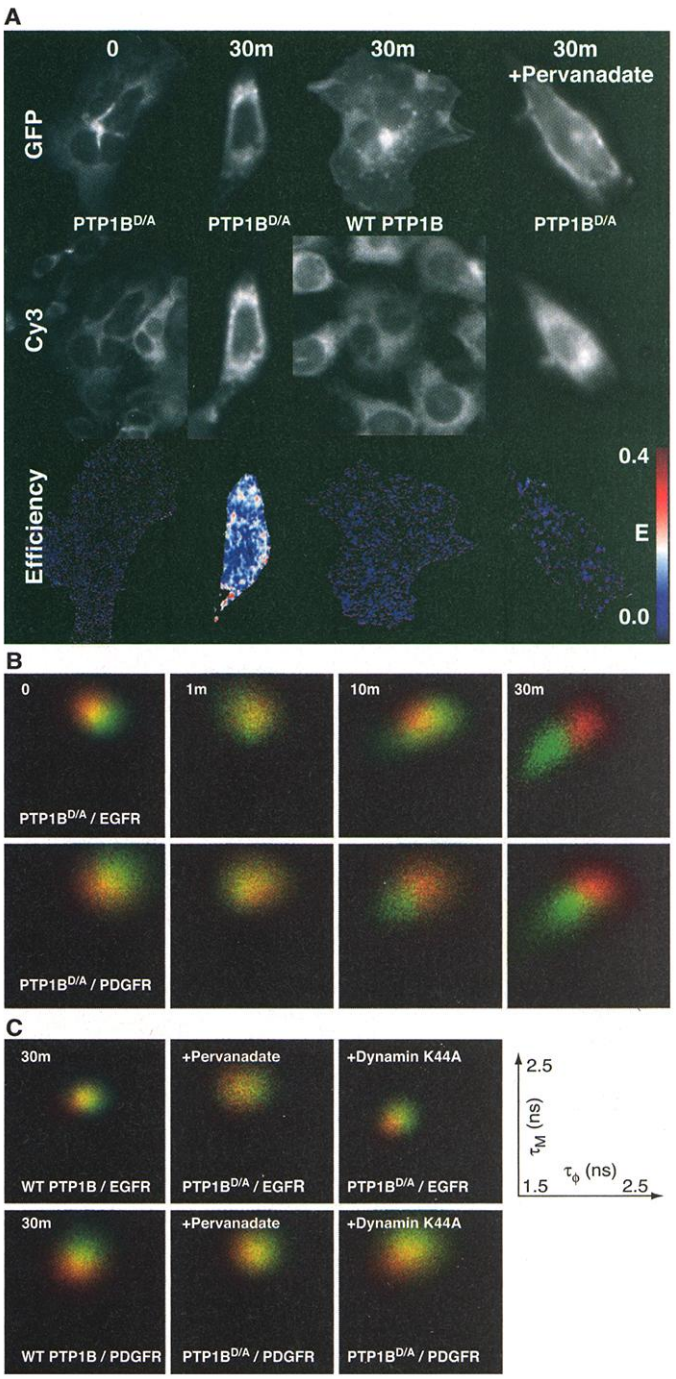

Fig. 2. PTP1B interacts with EGFR and PDFGR. FRET between EGFR-GFP or PDGFR-GFP and Cy3/FG6 was detected by FLIM (*19*). Cells were transfected with EGFR-GFP or PDGFR-GFP, stimulated as in Fig. 1, fixed in 4% formaldehyde, permeabilized in Triton X-100 (0.1%) and incubated with Cy3/FG6. (**A**) Images of interactions between PTP1B and EGFR. (Top panels) EGFR-GFP fluorescence intensity; (middle panels) Cy3/FG6 fluorescence intensity; (lower panels) FRET efficiency $E(i)$ at pixel i, as calculated from the phase lifetime estimation $\tau_\phi(i)$ by $E(i) = 1 - \tau_\phi(i)/\langle\tau_{\phi,D}\rangle$, where $\langle\tau_{\phi,D}\rangle$ is the average phase lifetime estimation obtained after photobleaching the acceptor. (Left to right) Unstimulated PTP1B$^{D/A}$-reconstituted cells; PTP1B$^{D/A}$-reconstituted cells, stimulated with EGF (100 ng/ml; 30 min); WT PTP1B-reconstituted cells, stimulated with EGF; PTP1B$^{D/A}$-reconstituted cells, stimulated with EGF and simultaneously incubated with pervanadate (1mM). Similar patterns were observed for PDGFR-GFP–transfected cells [Web fig. 2 (*13*)]. (**B**) Cumulative 2D histograms of phase (τ_ϕ) and modulation (τ_M) lifetimes before (green) and after (red) photobleaching the acceptor. (Top panels) EGF-stimulated cells. (Lower panels) Cells stimulated with PDGF (50 ng/ml). (**C**) FRET requires stable interaction between the PTP1B active center and endocytosed RTKs. (Left to right) WT PTP1B-reconstituted cells, pervanadate-treated PTP1B$^{D/A}$-reconstituted cells, and PTP1B$^{D/A}$-reconstituted cells coexpressing dynamin (K44A). For the latter experiments, PTP1B$^{D/A}$-reconstituted cells were plated on MatTek dishes (MatTek Corporation, Ashland, MA), coinjected with cytomegalovirus-driven expression vectors for dynamin K44A (25 ng/μl) and the indicated GFP-tagged RTK (25 ng/μl), stimulated, and fixed as above.

WT PTP1B was localized on ER membranes in growth factor–deprived cells [Fig. 1A; Web fig. 1 (*1, 13*)]. PTP1B$^{D/A}$ also exhibited a reticular staining pattern that colocalized with the ER marker translocon-associated protein alpha (TRAP-α) in growth factor–deprived cells [Fig. 1B; Web fig. 1 (*13*)] (*1*). Thus, inactivation of the PTP catalytic domain does not, a priori, alter PTP1B localization, consistent with earlier work identifying the COOH-terminal hydrophobic domain as necessary and sufficient for ER localization (*6*). Within 15 min of growth factor administration, cells reconstituted with PTP1B$^{D/A}$, but not those reconstituted with WT PTP1B, showed PTP1B immunoreactivity in discrete punctate structures that also immunostained with antibodies to TRAP-α [Fig. 1, C and D; Web fig. 1 (*13*)]. The majority of TRAP-α staining retained a reticular pattern under all conditions tested. Thus, PTP1B$^{D/A}$ expression does not alter ER integrity after growth factor stimulation; instead, PTP1B$^{D/A}$ appears to cluster in specific ER regions.

These observations suggested that PTP1B$^{D/A}$ might be clustered within the plane of the ER membrane, perhaps by interaction with endocytosed RTKs. Consistent with this notion, the punctate structures containing PTP1B$^{D/A}$ were immunoreactive with anti-phosphotyrosine antibodies (*5*). To directly assess PTP1B$^{D/A}$-RTK interactions at the molecular level, we measured FRET between EGFR-GFP or PDGFR-GFP and Cy3-FG6 by fluorescence lifetime imaging microscopy (FLIM) (*14–16*). FLIM is a robust method for measuring FRET in cells, because fluorescence lifetimes are independent of fluorophore concentration and light path length but dependent on excited-state reactions such as FRET (*17*). Also, FLIM data acquisition times are on the order of seconds, enabling a sufficiently high sample throughput to obtain reliable statistics on cell-to-cell variations (*18*). FRET between the GFP on the RTKs and the Cy3 acceptor on the anti-PTP1B antibodies was detected by a decrease in the fluorescence lifetime of the donor GFP fluorophore (*19*). Two images of different fluorescence lifetime estimations for GFP were computed from the FLIM data. In each pixel, the phase lifetime (τ_ϕ) was calculated from the phase shift of the sinusoidally modulated fluorescent light (*14*, *16*), and the modulation lifetime (τ_M) was calculated from its demodulation. Both lifetime estimations should decrease in areas of the cell where FRET occurs. After acquiring each FLIM data set, Cy3 was photobleached to obtain the control fluorescence lifetimes of the donor fluorophore (GFP) in the absence of the acceptor in the same sample (*20*). By plotting the cumulative two-dimensional (2D) histograms of τ_ϕ and τ_M for several samples under each experimental condition, the presence of FRET, and thus of RTK-PTP1B interactions, was detected easily by the increase in fluorescence lifetimes after photobleaching (red dots in Fig. 2, B and C), compared with those in unbleached samples (green dots). Overlap (yellow) between the pre- and postbleached distributions represents absence of FRET. From the fluorescence lifetime measurements before and after photobleaching, the apparent energy transfer efficiency also was calculated at each pixel of the image (Fig. 2A).

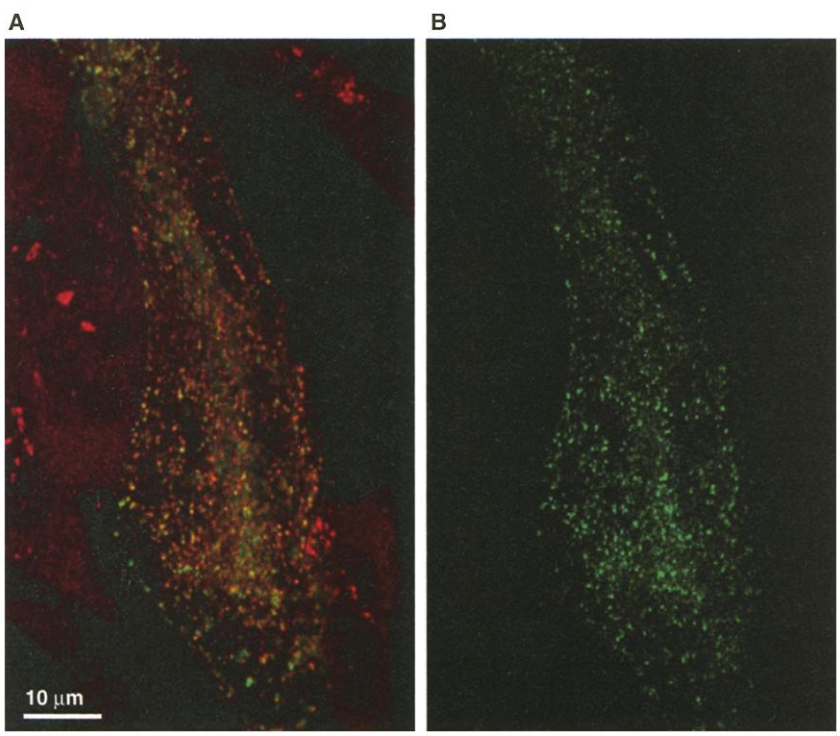

Fig. 3. High-resolution 3D map of the interaction between the EGFR and PTP1B. FRET was detected by using the acceptor photobleaching approach. Samples were prepared as in Fig. 2, and images were acquired with a confocal laser scanning microscope (Leica TCS SP2, Leica, Wetzlar, Germany) equipped with a 63×/1.3 NA oil immersion lens, by using the 488-nm line of an Ar laser (GFP) and the 543-nm line of a HeNe laser (Cy3). Specific photobleaching of the acceptor was accomplished by extensive illumination (10 to 15 min) with the HeNe laser. Stacks of images of the donor (EGFR-GFP) and acceptor (Cy3/FG6) were acquired before and after photobleaching. After deconvolution of the GFP images by using the Huygens program (Scientific Volume Imaging BV, Hilversum, Netherlands), and registration by correlation, the difference was calculated in each voxel (a 3D representation of a pixel), which is directly proportional to the concentration of donor molecules in a complex that exhibits FRET. The images shown are projections of the maximum intensity along the axial *z* direction. (**A**) Colocalization of donor (green) and acceptor (red) fluorescence intensities before photobleaching in cells stimulated for 30 min with EGF. (**B**) Difference images of the donor fluorescence intensity before and after acceptor photobleaching, showing that the punctate structures exhibit FRET. Comparable patterns were observed for PDGFR-GFP–transfected cells [Web fig. 3 (*13*)]. For movies of 3D-rendered colocalization and difference images, see supplementary material (*13*).

FRET was not observed in cells reconstituted with WT PTP1B [Fig. 2, A and C; Web fig. 2 (*13*)] at any time after growth factor stimulation, probably because of the small amounts of enzyme-substrate complexes at steady state. Likewise, no interactions between PTP1B$^{D/A}$ and the PDGFR or EGFR were apparent in resting cells or in cells that were stimulated for short times (1 min) with the cognate growth factor (Fig. 2B). However, at 10 and 30 min after growth factor administration, punctate structures in which FRET could be detected were visible, indicative of localized interactions between the RTKs and PTP1B$^{D/A}$ [Fig. 2, A and B; Web fig. 2 (*13*)]. Prior treatment of the cells with pervanadate, which inhibits PTPs by binding to and modifying the essential catalytic cysteinyl residues at their active sites (*21*), led to the disappearance of the punctate structures and completely abolished FRET [Fig. 2, A and C; Web fig. 2 (*13*)]. These data show that the interactions visualized by FRET require the PTP1B catalytic center and therefore represent sites at which RTK dephosphorylation occurs within the cell.

The punctate structures were more apparent and FRET was more efficient 30 min after stimulation, which suggested that the RTKs were interacting with PTP1B after endocytosis (Fig. 2, A and B). To test this hypothesis directly, we assessed the effects of a dominant-negative mutant of dynamin (K44A), in which lysine 44 is replaced by an alanine. Dynamin is a guanosine triphosphatase (GTPase) that controls the formation of constricted coated pits (*22*). The K44A mutant lacks GTPase activity and blocks ligand-induced endocytosis of RTKs (*23*). K44A expression decreased FRET between the RTKs

and PTP1B$^{D/A}$, even in cells stimulated for 30 min with EGF or PDGF (Fig. 2C).

The data above indicated that after growth factor stimulation, PTP1B interacts with internalized RTKs [Fig. 2; Web fig. 2 (*13*)]. To determine whether RTK-PTP1B interactions occur within the punctate structures we observed in the ER, we generated a high-resolution 3D image of the sites of RTK-PTP1B interaction in cells. We monitored localization of these molecules by confocal microscopy (Fig. 3A) and their interactions by FRET using the acceptor photobleaching approach (Fig. 3B), which measures the increased intensity of a donor fluorophore that follows photobleaching of the acceptor (*24*). After 30 min of growth factor stimulation, high FRET efficiencies were observed exclusively on the punctate structures [Fig. 3B; Web fig. 3 and movies 1 and 2 (*13*)], where PTP1B and the RTKs colocalize [Fig. 3A; Web fig. 3 and movies 1 and 2 (*13*)].

Thus, RTK interactions with the catalytic center of PTP1B—and, by inference, RTK dephosphorylation by PTP1B—require receptor endocytosis, occur at specific times after growth factor activation, and take place in discrete spatial locations within the cell. ER-anchored PTP1B specifically dephosphorylates endocytosed RTKs, thereby contributing to RTK signal termination. Other PTPs may function at the plasma membrane to prevent gratuitous RTK activation or activation by subthreshold levels of growth factor. Ligand-induced RTK activation overcomes these local PTPs, possibly by promoting the production of reactive oxygen species that can transiently oxidize the essential catalytic cysteinyl residue in PTPs (*25*). Receptor endocytosis also may play an important role in potentiating RTK activation, by promoting separation between RTKs and plasma membrane–proximal PTPs. Although PTPs play a critical role in RTK signal modulation, specific seryl phosphorylation events (*26*) and RTK targeting to lysosomes, a process that involves RTK ubiquitination (*27*, *28*), also are important RTK-inactivation mechanisms. From our FLIM data, we estimate that about 20% of all the EGFR-GFP molecules in a cell exhibit FRET with PTP1B (at 30 min after EGF stimulation). About 35% of total EGFR-GFP molecules are active under similar conditions (*18*). Taken together, these data imply that a high percentage of activated RTKs become associated with PTP1B$^{D/A}$. Therefore, consistent with a recent study showing that EGFR inactivation precedes degradation (*29*), our data show that most, if not all, incoming RTKs transit a "dephosphorylation compartment" before targeting to the lysosome or recycling to the plasma membrane. Functional imaging techniques such as those presented here should permit further elucidation of the spatiotemporal organization of PTP function and help us to understand how, where, and when these other negative regulatory processes function within the cell.

References and Notes

1. A. J. Flint, T. Tiganis, D. Barford, N. K. Tonks, *Proc. Natl. Acad. Sci. U.S.A.* **94**, 1680 (1997).
2. B. J. Goldstein, F. Ahmad, W. Ding, P. M. Li, W. R. Zhang, *Mol. Cell. Biochem.* **182**, 91 (1998).
3. M. Elchebly *et al.*, *Science* **283**, 1544 (1999).
4. L. D. Klaman *et al.*, *Mol. Cell. Biol.* **20**, 5479 (2000).
5. F. G. Haj, B. G. Neel, unpublished data.
6. J. V. Frangioni, P. H. Beahm, V. Shifrin, C. A. Jost, B. G. Neel, *Cell* **68**, 545 (1992).
7. T. A. Woodford-Thomas, J. D. Rhodes, J. E. Dixon, *J. Cell Biol.* **117**, 401 (1992).
8. Z. Y. Zhang, D. Maclean, D. J. McNamara, T. K. Sawyer, J. E. Dixon, *Biochemistry* **33**, 2285 (1994).
9. J. B. Bliska, J. C. Clemens, J. E. Dixon, S. Falkow, *J. Exp. Med.* **176**, 1625 (1992).
10. N. K. Tonks, B. G. Neel, *Curr. Opin. Cell Biol.* **13**, 182 (2001).
11. A. J. Garton, A. J. Flint, N. K. Tonks, *Mol. Cell. Biol.* **16**, 6408 (1996).
12. Primary mouse embryonic fibroblasts were generated from day 14 PTP1B-deficient mouse embryos and immortalized by infection with a retroviral vector expressing SV40 large T antigen. Immortalized PTP1B$^{-/-}$ cells were subsequently reconstituted with WT or D181A PTP1B cloned into the retroviral vector, pWZL Hygro. Pools of hygromycin-resistant cells, over 95% of which express PTP1B (as revealed by immunostaining), were used for the experiments. All cells were cultured in Dulbecco's modified Eagle's medium supplemented with 10% fetal calf serum, penicillin (100 U/ml), and streptomycin (10 mg/ml).
13. Supplementary material is available on *Science* Online at www.sciencemag.org/cgi/content/full/295/5560/1708/DC1.
14. T. W. J. Gadella Jr., T. M. Jovin, R. M. Clegg, *Biophys. Chem.* **48**, 221 (1993).
15. J. R. Lakowicz, K. Berndt, *Rev. Sci. Instrum.* **62**, 1727 (1991).
16. A. Squire, P. I. H. Bastiaens, *J. Microsc.* **193**, 36 (1999).
17. P. I. H. Bastiaens, A. Squire, *Trends Cell Biol.* **9**, 48 (1999).
18. P. J. Verveer, F. S. Wouters, A. R. Reynolds, P. I. H. Bastiaens, *Science* **290**, 1567 (2000).
19. FLIM sequences were obtained at a modulation frequency of 80 MHz with an Olympus IX70 microscope, using a 100×/1.4 numerical aperture (NA) oil objective. GFP was excited with a 476-nm Argon laser line, and fluorescence was detected with a dichroic beamsplitter (Q495 LP; Chroma Technology, Brattleboro, VT) and a narrow-band emission filter (HQ510/20; Chroma). Cy3 images were recorded with a 100-W Mercury arc lamp with a high Q Cy3 filter set (excite: HQ 545/30; dichroic: Q 580 LP; emitter: HQ 610/75).
20. F. S. Wouters, P. I. H. Bastiaens, *Curr. Biol.* **9**, 1127 (1999).
21. G. Huyer *et al.*, *J. Biol. Chem.* **272**, 843 (1997).
22. S. Sever, H. Damke, S. L. Schmid, *J. Cell Biol.* **150**, 1137 (2000).
23. A. V. Vieira, C. Lamaze, S. L. Schmid, *Science* **274**, 2086 (1996).
24. P. I. H. Bastiaens, I. V. Majoul, P. J. Verveer, H.-D. Söling, T. M. Jovin, *EMBO J.* **15**, 4246 (1996).
25. T. Finkel, *FEBS Lett.* **476**, 52 (2000).
26. J. Schlessinger, *Cell* **103**, 211 (2000).
27. G. Levkowitz *et al.*, *Mol. Cell* **4**, 1029 (1999).
28. C. A. Joazeiro *et al.*, *Science* **286**, 309 (1999).
29. P. Burke, K. Schooler, H. S. Wiley, *Mol. Biol. Cell* **12**, 1897 (2001).

30. We thank N. Tonks (Cold Spring Harbor Laboratory, NY) for PTP1B-expressing retroviral vectors, S. Schmid (Scripps Institute, CA) for the dominant-negative dynamin mutant, T. Rapoport and M. Rolls (Harvard Medical School) for anti-TRAPα antibodies and helpful discussions, V. Georget [European Molecular Biology Laboratory (EMBL), Heidelberg] for the PDGFR-GFP construct, and R. Saffrich (EMBL, Heidelberg) for help with microinjection of cells. We also thank L. Cantley and C. Carpenter for critical comments on the manuscript. This work was supported by NIH grant R01 CA49152 (to B.G.N.). F. Haj was aided by a mini-sabbatical award from the Harvard Digestive Diseases Center and P. Verveer was supported by a Marie Curie Fellowship of the European Community.

30 October 2001; accepted 9 January 2002

Discrete Microdomains with High Concentration of cAMP in Stimulated Rat Neonatal Cardiac Myocytes

Manuela Zaccolo* and Tullio Pozzan

The second messenger cyclic adenosine monophosphate (cAMP) is the most important modulator of sympathetic control over cardiac contractility. In cardiac myocytes and many other cell types, however, cAMP transduces the signal generated upon stimulation of various receptors and activates different cellular functions, raising the issue of how specificity can be achieved. In the general field of signal transduction, the view is emerging that specificity is guaranteed by tight localization of signaling events. Here, we show that in neonatal rat cardiac myocytes, β-adrenergic stimulation generates multiple microdomains with increased concentration of cAMP in correspondence with the region of the transverse tubule/junctional sarcoplasmic reticulum membrane. The restricted pools of cAMP show a range of action as small as approximately 1 micrometer, and free diffusion of the second messenger is limited by the activity of phosphodiesterases. Furthermore, we demonstrate that such gradients of cAMP specifically activate a subset of protein kinase A molecules anchored in proximity to the T tubule.

cAMP has been regarded as a freely diffusible second messenger (*1*) that mediates the action of a number of different receptors and modulates many cellular functions, as diverse as movement, growth, metabolism, and synaptic plasticity. In the heart, cAMP generated upon β-adrenergic receptor (β-AR) stimulation controls strength, duration, and frequen-